Supplementary Information for

Achieving Pt Coating-Free Anodes Using Double-Layered Catalyst Layer Structure for Polymer Electrolyte Membrane Water Electrolysis

Daehee Kim,[a,b] Gi Hong Jung,[a] Young Hwa Yun,[a] Jeesoo Park,[c] Sieon An,[a] Changsoo Lee,[a] Sechan Lee,[d,e] Hyeonjung Park,[a] Sang-Kyung Kim,[a] Hyun-Seok Cho,[f] Hee-Tak Kim,[c] Namgee Jung,[b] Gisu Doo,[a]* MinJoong Kim.[g]**

[a]Hydrogen Research Department, Korea Institute of Energy Research (KIER), 152 Gajeong-ro, Yuseong-gu, Daejeon 34129, Republic of Korea

[b]Graduate School of Energy Science and Technology (GEST), Chungnam National University, 99 Daehak-ro, Yuseong-gu, Daejeon 34134, Republic of Korea

[c]Department of Chemical and Biomolecular Engineering, Korea Advanced Institute of Science and Technology (KAIST), 291 Daehak-ro, Yuseong-gu, Daejeon 34141, Republic of Korea

[d]Department of Chemistry, Kookmin University, 77 Jeongneung-ro, Seongbuk-gu, Seoul 02707, Republic of Korea

[e]Department of Applied Chemistry, 77 Jeongneung-ro, Seongbuk-gu, Kookmin University, Seoul 02707, Republic of Korea

[f]Department of Chemical and Biomolecular Engineering, Sogang University, 35 Baekbeom-ro, Mapo-gu, Seoul 04107, Republic of Korea

[g]Department of Materials Science and Engineering, Kyung Hee University, 1732 Deogyeong-daero, Giheung-gu, Yongin, Gyeonggi-do 17104, Republic of Korea

*E-mail: (N. Jung) njung@cnu.ac.kr (G. Doo) dooanything@kier.re.kr (M.J. Kim) mj.kim@khu.ac.kr

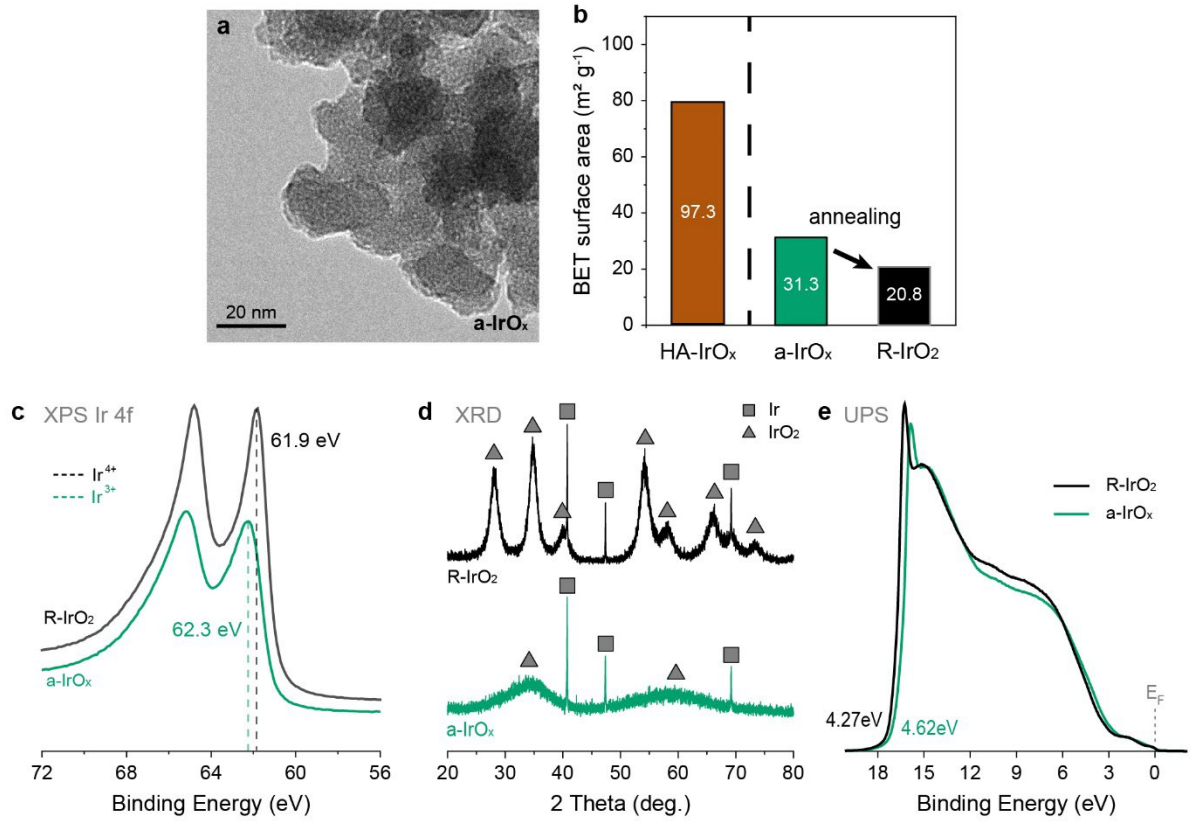

Fig. S1. Structural and electronic characterization of the amorphous (a-IrO$_x$) and rutile (R-IrO$_2$) catalysts. (a) TEM images of the a-IrO$_x$ catalysis. (b) Microstructure comparison of the catalysts using BET methods. (c–e) Electronic and structural analysis using (c) XPS Ir 4f spectra, (d) XRD plots, and (e) UPS spectra.

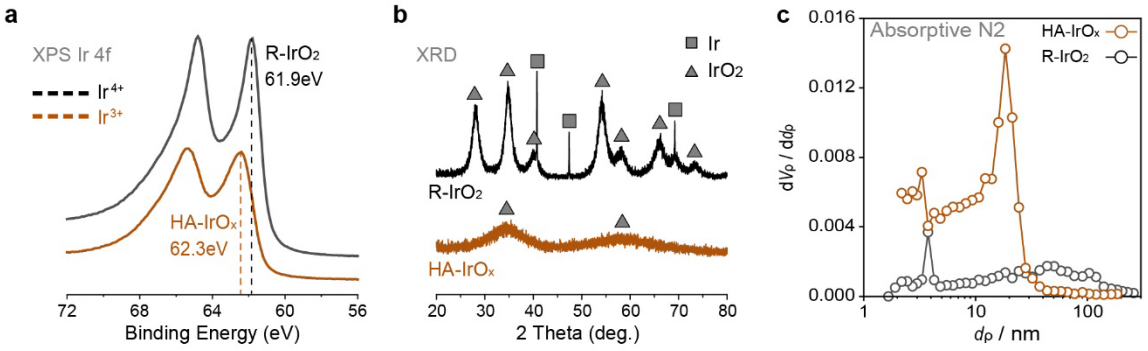

Fig. S2. Structural and electronic characterizations of the HA-IrO$_x$ and R-IrO$_2$ catalysts. (a) XPS Ir 4f spectra, (b) XRD plots, and (c) pore distribution analysis of the catalyst particles using the BJH method.

Supplementary Note 1.

In our study, the single-cell voltage was deconvoluted into kinetic, ohmic, and transport overpotentials using a combination of electrochemical impedance spectroscopy (EIS), polarization curve, and Tafel plot. We first assumed that the cathode contribution is negligible compared to that from the membrane and anode compartments. The single-cell voltage (E_{cell}) was deconvoluted based on the following expression:

$$E_{cell} = E_{rev} + \eta_{act} + i \cdot R_{ohm} + i \cdot R_{CL}^{eff} + \eta_{mass} \quad [1]$$

, where E_{rev} is the reversible voltage (1.18 V at 80 °C), and η_{act}, $i \cdot R_{ohm}$, $i \cdot R_{CL}^{eff}$, and η_{mass} are the overpotentials stemming from the OER kinetics, ohmic components, ion/electron transport in CL, and material transport of oxygen and water, respectively. Firstly, ohmic overpotential ($i \cdot R_{ohm}$) was determined from the high-frequency resistance (HFR or R_{ohm}) values obtained from the Nyquist plots, which include the contributions from the membrane and interfacial resistances (i.e., CL/PTL interface resistance). To isolate the kinetic overpotential (η_{act}), the iR-corrected polarization curve was plotted against the logarithm of current density, and the Tafel line was extrapolated from the linear region at low current densities (typically at the range of 40 – 100 mA cm^{-2}). The values obtained by subtracting the reversible voltage from the Tafel extrapolation were considered as the kinetic overpotential. Lastly, the remaining deviation between the iR-free curve and Tafel extrapolation, which is associated with mass transport overpotential (η_{mass}) and electron/ion transport within the tortuous anode CL ($i \cdot R_{CL}^{eff}$), was categorized as the "other" overpotential in this study.

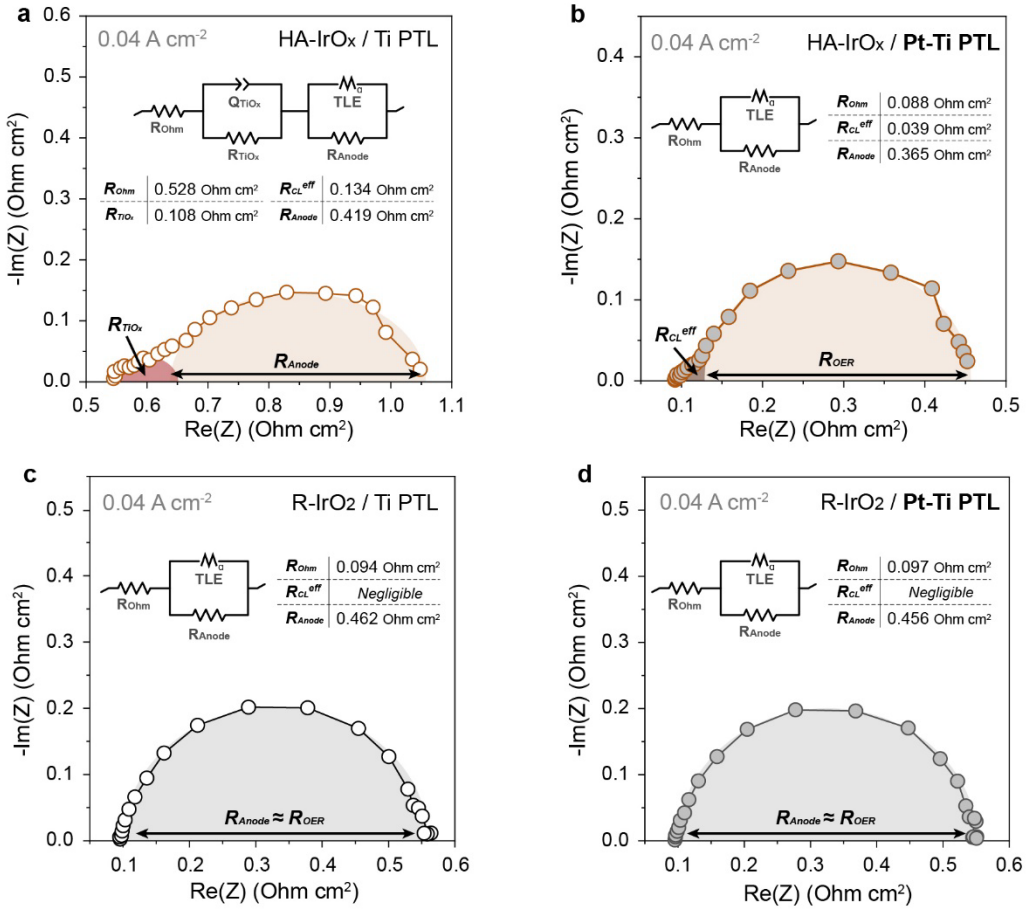

Fig. S3. Nyquist plots of single-layered anodes at 0.04 A cm^{-2} with the equivalent circuit model fitting. (a, b) HA-IrO_x-based anodes and (c, d) R-IrO_2-based anodes with (a, c) bare Ti PTL and (b, d) Pt-coated PTL.

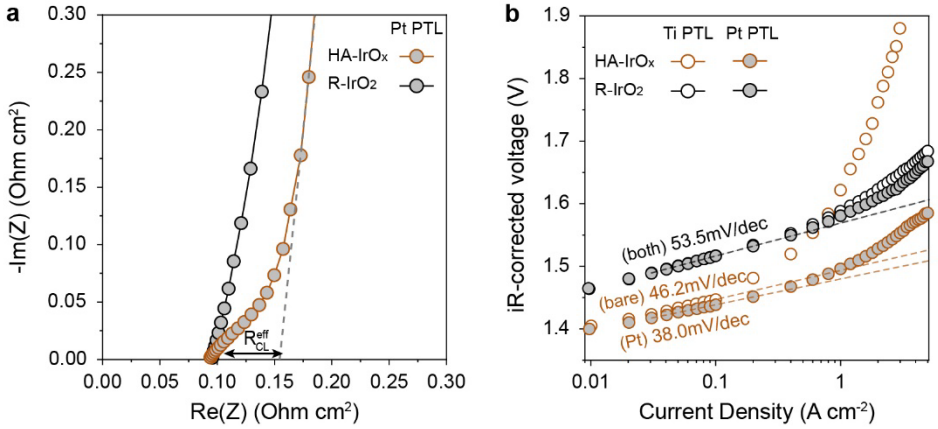

Fig. S4. Single-cell data comparisons of the HA-IrO_x and R-IrO_2 CLs. (a) Impedance analysis at 1.35 V and (b) Tafel plots.

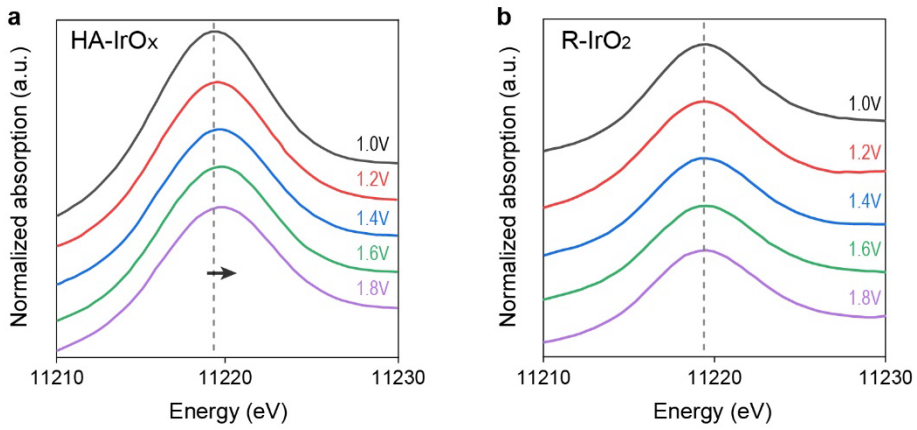

Fig. S5. X-ray Absorption Spectroscopy (XAS) analysis of the HA-IrO$_x$ and R-IrO$_2$ catalysts with varying applied potentials. (a) Ir L_3-edge XANES analysis of the HA-IrO$_x$ and (b) R-IrO$_2$ catalysts at a potential range of 1.0–1.8 V vs. RHE.

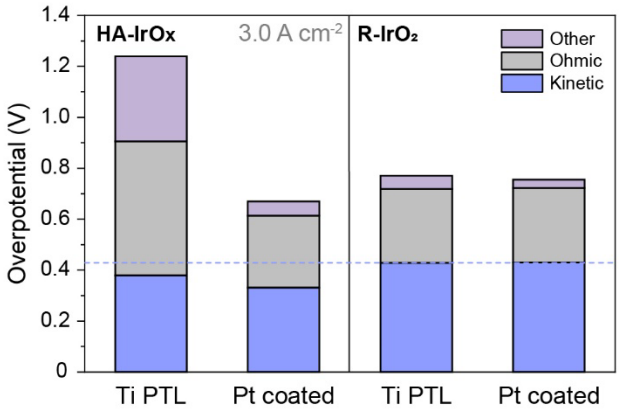

Fig. S6. Overpotential breakdown analysis at 3.0 A cm^{-2} for the two single-layered CLs depending on the Pt coating.

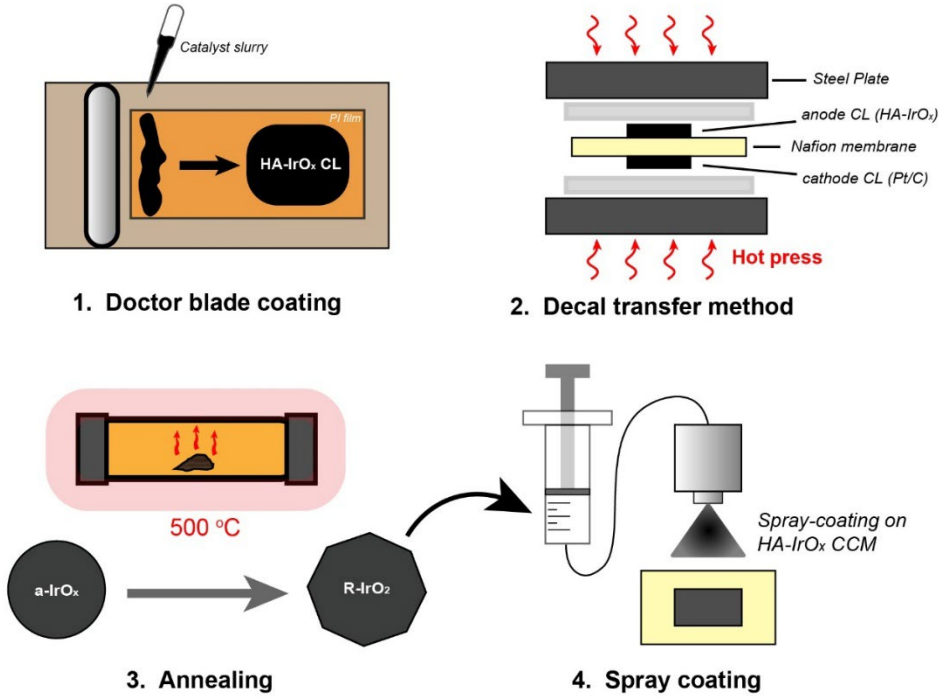

81

82 **Fig. S7.** Schematic illustrations of the fabrication processes for DL-CL.

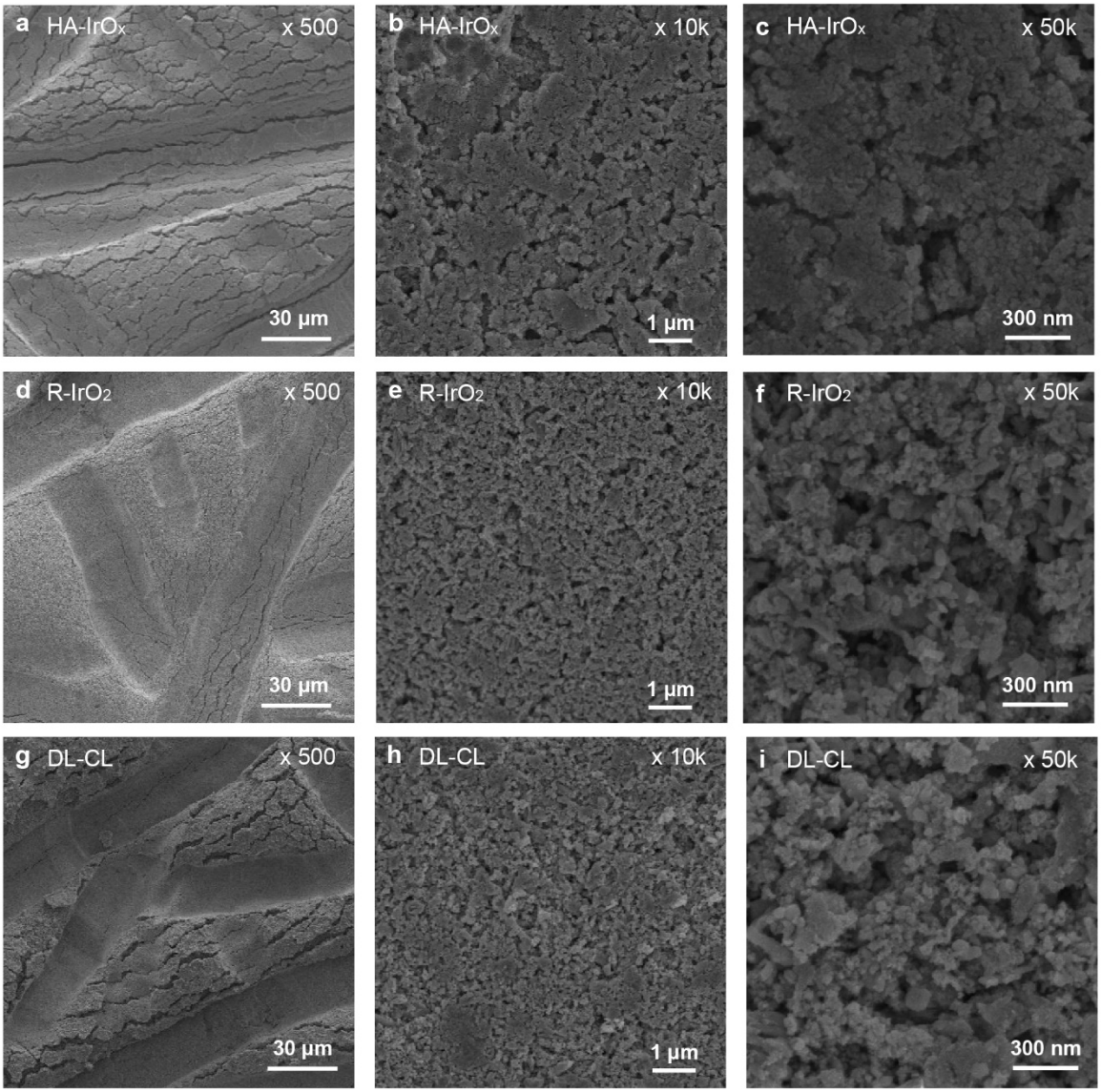

Fig. S8. Surface SEM images of the (a–c) HA-IrO_x, (d–f) R-IrO_2, and (g–i) DL-CL CCMs. At high magnifications, the DL-CL features surface morphology identical to that of the R-IrO_2 CCM.

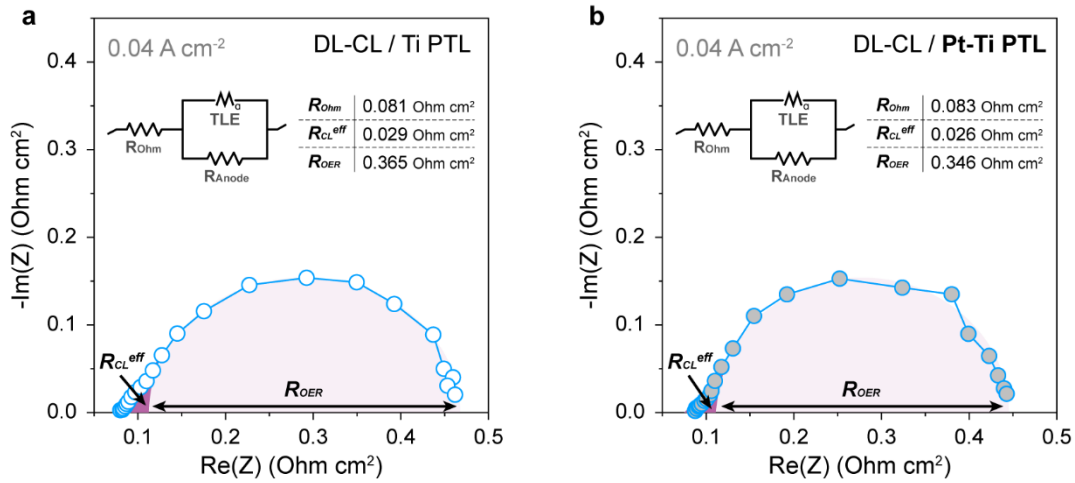

87

88 **Fig. S9.** Nyquist plots and the equivalent circuit model fitting of the DL-CL anodes at 0.04 A
89 cm^{-2} with (a) bare Ti PTL and (b) Pt-coated PTL.

90

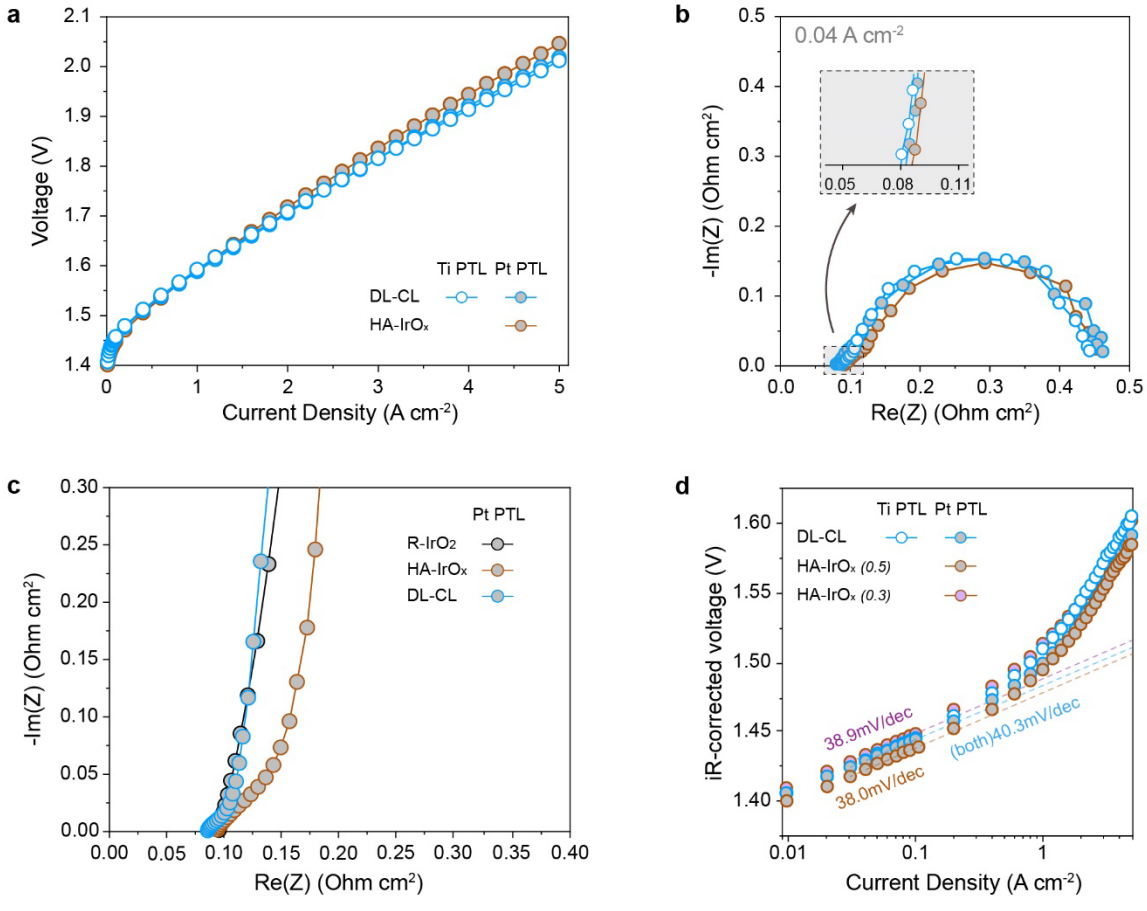

91

92 **Fig. S10.** (a) IV polarization curves and (b) Nyquist plots of the DL-CL anode with and without
93 the Pt coating. (c) Nyquist plots of the complex impedances at 1.35 V for the Pt-coated anodes.
94 (d) Tafel plots of the DL-CL anodes and the comparison with the HA-IrO_x anodes with two
95 different loadings (0.30 and 0.50 mg_{Ir} cm^{-2}).

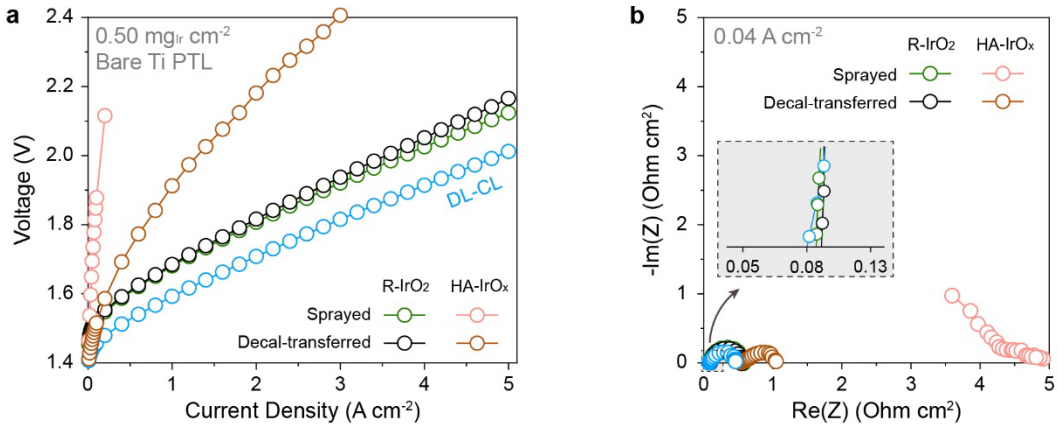

Fig. S11. (a) IV polarization curves and (b) Nyquist plots of the single-layered R-IrO_2 and HA-IrO_x CCMs fabricated via spray-coating and decal-transferring methods. All the CCMs were coupled with the bare Ti PTL.

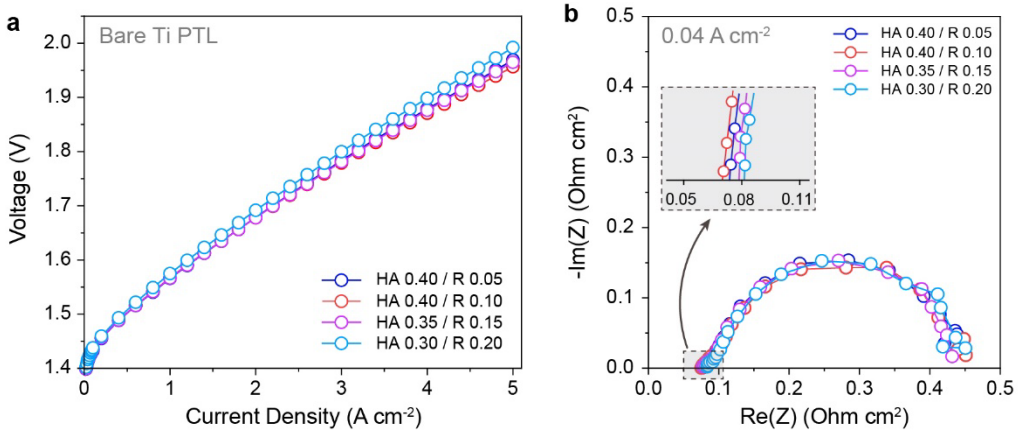

Fig. S12. R-IrO_2 catalyst loading effect for the DL-CL anode. (a) IV polarization curves and (b) Nyquist plots. The total loadings were controlled to 0.5 mg_{Ir} cm^{-2}, while the ratio of the two catalysts was varied.

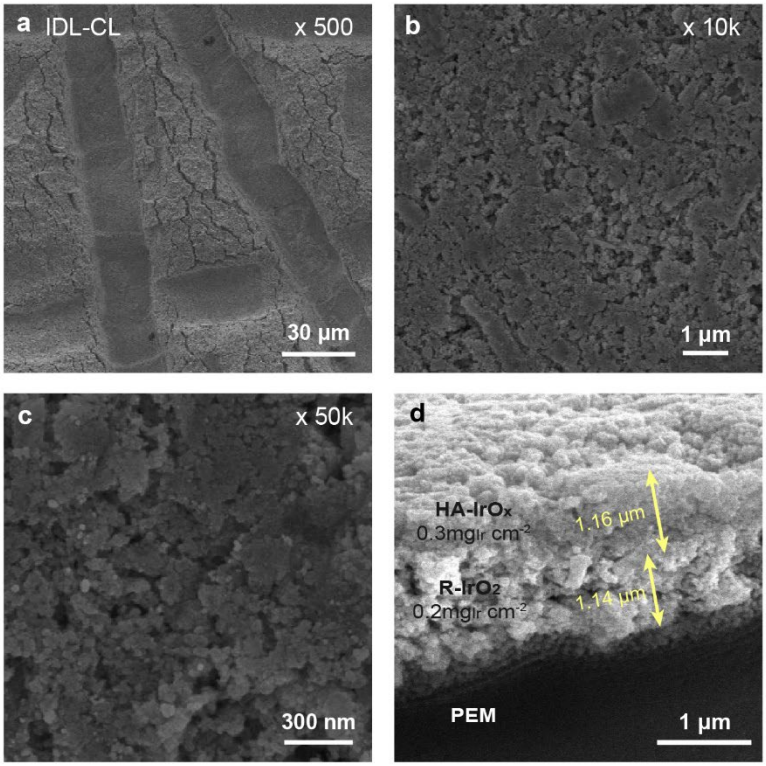

Fig. S13. (a–c) Surface and (d) cross-sectional SEM images of the IDL-CL CCM.

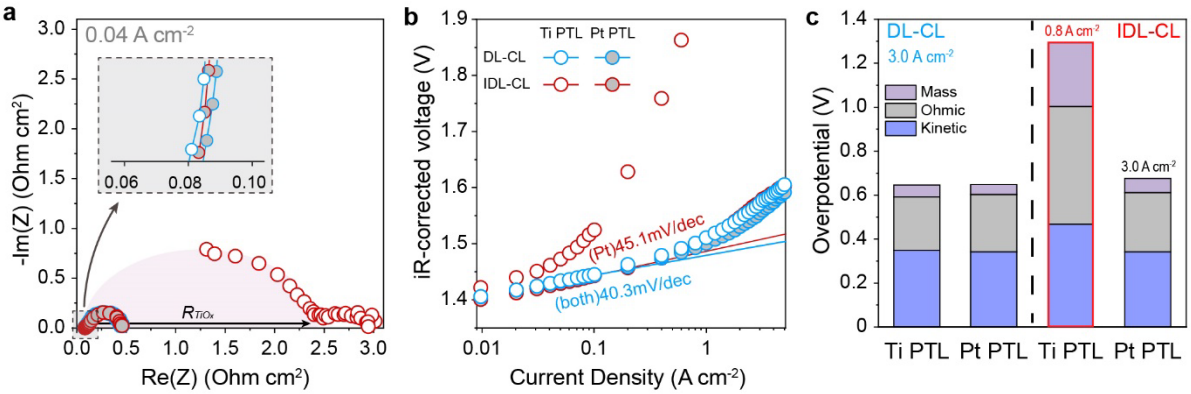

Fig. S14. Single-cell data comparison of the DL-CL and IDL-CL anodes depending on the Pt coating. (a) Nyquist plots at 0.04 A cm^{-2}, (b) Tafel plots, and (c) Overpotential breakdown at 3.0 A cm^{-2}.

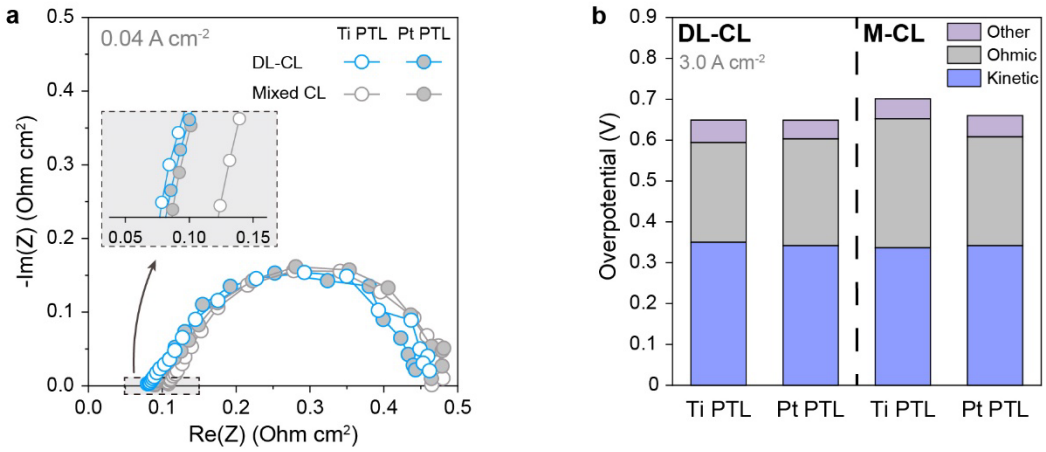

Fig. S15. Electrochemical analysis of the DL-CL and M-CL anodes depending on the Pt coating. (a) Nyquist plots at 0.04 A cm^{-2} and (b) Overpotential breakdown at 3.0 A cm^{-2}.

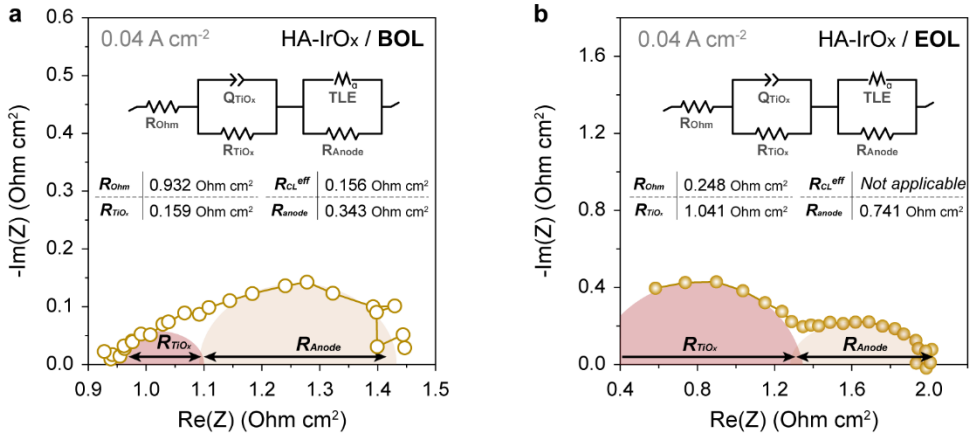

Fig. S16. Nyquist plots and their equivalent circuit model fitting of the HA-IrO_x anodes at 0.04 A cm^{-2} (a) before and (b) after the 1000h of constant current operation (1 A cm^{-2}).

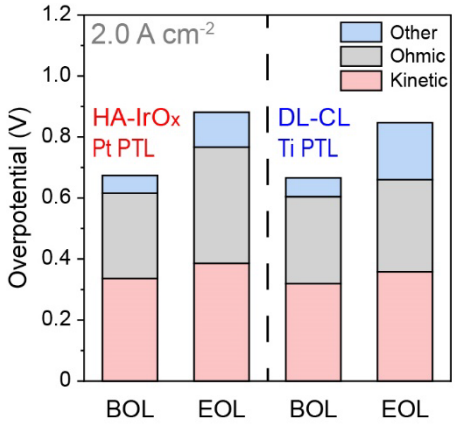

135

136 **Fig. S17.** Overpotential breakdown analysis at 2.0 A cm^{-2} of the HA-IrO_x (Pt-coated PTL) and
137 DL-CL (bare Ti PTL) before and after the long-term operation.